Using the ionospheric response to the solar eclipse on 20th March 2015 to detect spatial structure in the solar corona

PHILOSOPHICAL TRANSACTIONS A

rsta.royalsocietypublishing.org

Research

Cite this article: Scott CJ, Bradford J, Bell SA, Wilkinson J, Barnard L, Smith D, Tudor S. 2016 Using the ionospheric response to the solar eclipse on 20 March 2015 to detect spatial structure in the solar corona. *Phil. Trans. R. Soc. A* **374**: 20150216.
http://dx.doi.org/10.1098/rsta.2015.0216

Accepted: 12 January 2016

One contribution of 16 to a theme issue 'Atmospheric effects of solar eclipses stimulated by the 2015 UK eclipse'.

Subject Areas:
atmospheric science, geophysics

Keywords:
solar eclipse, ionosphere, tomography

Author for correspondence:
C. J. Scott
e-mail: chris.scott@reading.ac.uk

THE ROYAL SOCIETY PUBLISHING

Using the ionospheric response to the solar eclipse on 20 March 2015 to detect spatial structure in the solar corona

C. J. Scott[1], J. Bradford[2], S. A. Bell[3], J. Wilkinson[4], L. Barnard[1], D. Smith[5] and S. Tudor[5]

[1]Department of Meteorology, University of Reading, Earley Gate, PO Box 243, Reading RG6 6BB, UK
[2]RAL Space, Rutherford Appleton Laboratory, Chilton, Oxfordshire OX11 0QX, UK
[3]H.M. Nautical Almanac Office, UK Hydrographic Office, Admiralty Way, Taunton TA1 2DN, UK
[4]Zooniverse, c/o Astrophysics Department, University of Oxford, Oxford OX1 3RH, UK
[5]North Wales Astronomy Society, Colwyn Bay, UK

CJS, 0000-0001-6411-5649; LAB, 0000-0001-9876-4612

The total solar eclipse that occurred over the Arctic region on 20 March 2015 was seen as a partial eclipse over much of Europe. Observations of this eclipse were used to investigate the high time resolution (1 min) decay and recovery of the Earth's ionospheric E-region above the ionospheric monitoring station in Chilton, UK. At the altitude of this region (100 km), the maximum phase of the eclipse was 88.88% obscuration of the photosphere occurring at 9:29:41.5 UT. In comparison, the ionospheric response revealed a maximum obscuration of 66% (leaving a fraction, Φ, of uneclipsed radiation of $34 \pm 4\%$) occurring at 9:29 UT. The eclipse was re-created using data from the *Solar Dynamics Observatory* to estimate the fraction of radiation incident on the Earth's atmosphere throughout the eclipse from nine different emission wavelengths in the extreme ultraviolet (EUV) and X-ray spectrum. These emissions, having varying spatial distributions, were each obscured differently during the eclipse. Those wavelengths associated with coronal emissions (94, 211 and 335 Å) most closely reproduced the time varying fraction of unobscured radiation observed in

the ionosphere. These results could enable historic ionospheric eclipse measurements to be interpreted in terms of the distribution of EUV and X-ray emissions on the solar disc.

This article is part of the themed issue 'Atmospheric effects of solar eclipses stimulated by the 2015 UK eclipse'.

1. Introduction

The total solar eclipse visible over the Arctic region on 20 March 2015 gave observers across the UK an opportunity to witness a partial solar eclipse in which between 95% and 85% of the photosphere was obscured by the Moon, depending on the location of the observer. This was the greatest obscuration visible over the UK since the total solar eclipse over the southwest of England on 11 August 1999. During the 1999 solar eclipse, measurements were made of the Earth's ionosphere (the ionized portion of the Earth's upper atmosphere created when extreme ultraviolet (EUV) and X-ray radiation are absorbed by the neutral atmosphere at altitudes above 90 km). Historically, prior to the space age, such measurements were made in an attempt to remotely determine the composition of the upper atmosphere from the decay rate of the ionosphere in the absence of solar radiation [1]. An implicit assumption was made in these early observations that all ionizing radiation came from within the photosphere and so would be obscured at totality. It has since been shown that this is not the case [2], with the majority of such short-wavelength radiation being produced in the high-temperature solar corona. The rate of ionospheric decay during solar eclipses was lower than expected due to continued ion production since, even at totality, a significant proportion of the solar corona remains uneclipsed above the limb of the eclipsed photosphere. With the advent of rocketry in the 1950s, the composition of the upper atmosphere could be determined by direct measurements and so the practice of observing the ionosphere during solar eclipses for these purposes became redundant. Now that the chemistry of the Earth's upper atmosphere has been determined, the many ionospheric experiments conducted during eclipses from 1932 to date have been re-interpreted to study the variation in the size of the uneclipsed corona [3–5]. Details of these early ionospheric eclipse experiments were collated in 1956 [1] while a few previously unpublished sets of eclipse data are included in the appendices of more recent studies [3,4].

The 2015 eclipse provided a further opportunity to investigate the decay of the Earth's ionosphere, although this time the focus of the experiment was to compare the observed ionospheric changes with artificial eclipses created using data from the *Solar Dynamics Observatory* (*SDO*) [6] in order to determine whether it is possible to detect the obscuration of active regions within the solar corona by observing simultaneous changes to the rate of decay of charge in the Earth's ionosphere.

Routine ionospheric soundings have been made in the UK since 20 September 1932, initially at the Radio Research Station at Ditton Park near Slough and subsequently at the Rutherford Appleton Laboratory in Chilton, Oxfordshire, UK [7]. Short-wave (1 MHz to approx. 20 MHz) radio pulses are transmitted and received at the same location. These measurements exploit the fact that the resonant frequency of ionospheric electrons (f, Hz) is proportional to the square-root of the electron concentration (N, m^{-2}) with the relation $f \approx 9\sqrt{N}$. A radio signal is returned from the ionosphere when the frequency of the radio pulse matches the resonant frequency of the local electrons. Since the density of ionization varies with height due to the relative extent with which solar radiation over the EUV and X-ray spectrum can penetrate the atmosphere, a height profile of ionization can be built up by transmitting short-wave radio pulses over a range of frequencies corresponding to the range of ionospheric resonant frequencies. The data are displayed as plots of time of flight against radio frequency known as ionograms. By assuming that the radio pulses travel at the speed of light in free space, the height can be estimated from the time of flight. These 'virtual heights' are overestimates for all but the lowest frequencies, however, since the atmosphere is weakly ionized, slowing the speed of the signal due to its resonance with the local

electrons. The electron concentration of each layer can be accurately determined by recording the highest frequency returned from each layer. The equipment used has varied from analogue equipment recording the data directly onto film to a modern digital sounder or 'Digisonde' in which the data are stored electronically and made available via the UK Solar System Data Centre (UKSSDC, www.ukssdc.ac.uk).

At the height of the ionospheric E-region (approx. 100 km), the atmosphere is dominated by molecular ions and neutral gases such that the rate of change of ionization is of the form

$$\frac{\mathrm{d}N}{\mathrm{d}t} = q - \alpha N^2, \tag{1.1}$$

where N is the electron concentration (m^{-3}), t is time in seconds, q is the ionization production rate ($\mathrm{m}^{-3}\,\mathrm{s}^{-1}$) and α is the loss rate of ionization ($\mathrm{m}^3\,\mathrm{s}^{-1}$). The production rate q is proportional to the intensity of the incoming solar radiation and, to a first approximation, varies with the cosine of the solar zenith angle.

Atmospheric constituent gases can be ionized by X-ray and EUV emissions, where the energy of the ionizing photon exceeds the threshold ionization energy [8]. At altitudes of the ionospheric E-region (approx. 100 km), the composition of the neutral thermosphere is dominated by molecular species (O_2 and N_2). When sunlit, the primary ionization mechanism of these ions is through photoionization and the dominant loss mechanism is through dissociative recombination with free electrons [8].

During an eclipse, the fraction, Φ, of ionizing radiation reaching the top of the atmosphere varies throughout, being a minimum around the time of maximum obscuration of the corona. Since the radiation from the solar corona is not distributed evenly, this may not correspond to the time of maximum eclipse for the photosphere. Equation (1.1) can then be rewritten as

$$\frac{\mathrm{d}N_\mathrm{E}}{\mathrm{d}t} = \Phi q - \alpha N_\mathrm{E}^2, \tag{1.2}$$

where the subscript E refers to the eclipse day. While equation (1.2) holds to first order, it contains the implicit assumption that the production and loss rates are not affected by any changes to thermospheric composition or temperature throughout the solar eclipse. At E-region altitudes, the primary loss mechanism is via dissociative recombination. This loss process is weakly dependent on the electron temperature. The lifetime of individual ions at this altitude is of the order of seconds and so transport of ionization is not significant. By comparing the electron density observed during the day of the eclipse with equivalent times from a control (in our case, modelled values in which there is no eclipse), it is possible to estimate Φ by combining equations (1.1) and (1.2):

$$\Phi = \frac{\mathrm{d}N_\mathrm{E}/\mathrm{d}t + \alpha N_\mathrm{E}^2}{\mathrm{d}N/\mathrm{d}t + \alpha N^2}. \tag{1.3}$$

In practice, the rates of change of ionization are sufficiently slow that, to a first-order approximation, they can be ignored, allowing the fraction of ionizing radiation to be expressed as

$$\Phi = \frac{N_\mathrm{E}^2}{N^2}. \tag{1.4}$$

By measuring the critical frequencies throughout the day of the eclipse and comparing these to a control, it becomes possible to estimate the fraction of ionizing radiation incident on the upper atmosphere during the eclipse. The aim of this study was to determine whether the structured emissions within the solar corona could be detected through changes to the decay rate of the Earth's ionosphere.

During this eclipse, the distribution of emissions across a variety of wavelengths within the X-ray and EUV section of the solar spectrum were monitored from the *SDO* [6]. The Atmospheric Imaging Assembly (AIA) instrument [9] on board the *SDO* makes high-cadence (2 min) full-sun images at wavelengths corresponding to specific emissions in the X-ray and EUV section of the electromagnetic spectrum. Each wavelength is associated with an emission from plasma at a

Table 1. Ion emissions monitored by the AIA instrument on board the *SDO* (adapted from table 1, Lemen *et al.* [9]). Emissions are ordered in ascending characteristic temperature (where there are two distinct temperatures associated with a given wavelength, the lower is used).

channel (Å)	primary ion(s)	region of atmosphere	characteristic temperature, log(T)
4500	continuum	photosphere	3.7
1700	continuum	temperature minimum, photosphere	3.7
304	He II	chromosphere, transition region	4.7
1600	C IV + continuum	transition region, upper photosphere	5.0
131	Fe VIII, XXI	transition region, flaring corona	5.6, 7.0
171	Fe IX	quiet corona, upper transition region	5.8
193	Fe XII, XXIV	corona and hot flare plasma	6.2, 7.3
211	Fe XIV	active-region corona	6.3
335	Fe XVI	active-region corona	6.4
94	Fe XVIII	flaring corona	6.8

specific temperature within the Sun's atmosphere. Nine of these wavelengths, ranging from 94 to 1700 Å, are considered here (the tenth, at 4500 Å, is not used, as the cadence at this wavelength was not sufficient during the eclipse period). These wavelengths, along with the effective temperature and emission species in the solar plasma, are presented in table 1. The effective temperatures covered by these emissions range from 5012 K to 19 950 000 K.

Solar EUV and X-ray emissions on the day of the eclipse, as measured by AIA on *SDO*, are presented in figure 1. When viewed in X-ray or shorter EUV wavelengths, emissions reveal two active regions on the limb adjacent to the southeast and southwest quadrants of the solar disc. The distribution of emissions varies between wavelengths, with those originating in the photosphere revealing more uniform emissions, with no significant emissions beyond the limb of the disc. It should be expected, therefore, that the fraction of ionizing radiation incident on the Earth's atmosphere at each of these wavelengths will differ from each other throughout the eclipse.

2. Method

The solar eclipse that occurred on the morning of 20 March 2015 was not total in the ionosphere above Chilton. As viewed from this vantage point, the Moon crossed the solar disc from right to left, leaving the solar south pole exposed throughout. First contact was at 8:23:28 UT, last contact was at 10:40:04 UT, with maximum eclipse (88.88%) occurring at 9:29:41 UT. The locations of the analogous positions at ground level are shown in figure 2 as a dotted line. Larger dots are plotted at intervals of 15 min. Owing to the rotation of the Earth, this location tracks across the surface during the morning of the eclipse, with first contact occurring over central Ireland (square symbol), peak eclipse over the North Wales coast (triangular symbol) and last contact near Chester (rightmost dot). For comparison, local circumstances for Bangor (53.22° N, 4.128° W), a town on the North Wales coast (indicated by the '×' in figure 2), were: first contact 08:25:00 UT, last contact 10:38:49 UT, with maximum eclipse (90.03%) occurring at 9:29:57 UT. In order to obtain ground truth for the ionospheric observations above Chilton, members of the North Wales Astronomy Society photographed the Sun through telescopes fitted with narrow-band filters centred on the Hα emission (656.281 nm). Such images enable large-scale features such as prominences and filaments within the solar atmosphere to be imaged. Observations were made from Trelawnyd (53.3069° N, 3.3659° W), which is represented by a '∗' symbol in figure 2. Comparing images taken from ground-based observers with simulated eclipses using *SDO* data provides a useful check on the analysis. The position of the ionospheric observatory at Chilton is represented by a diamond symbol in figure 2.

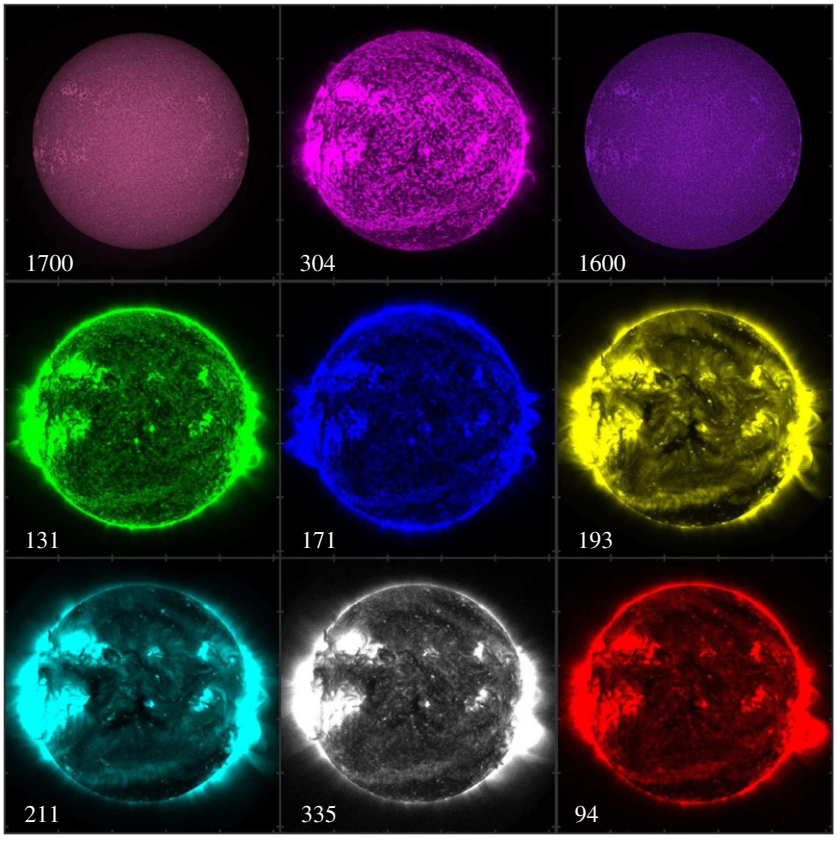

Figure 1. The Sun imaged in nine wavelengths in the EUV and X-ray spectrum by the AIA on the *SDO*. Each image is labelled with the wavelength of the emission (in ångström). The colour coding of each image has been chosen to match the colours of the curves in figure 5. These images represent the emissions at 10 UT on the morning of the eclipse. The distribution of emissions did not change significantly throughout the course of the eclipse.

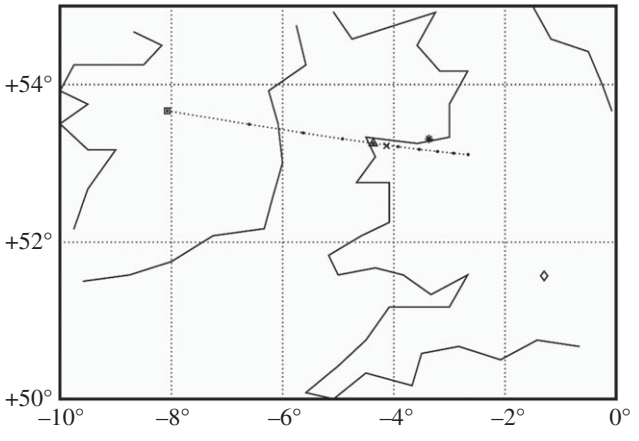

Figure 2. A map of the UK and Ireland showing the path (dotted line) of the ground-level location where the eclipse obscuration was analogous to that at 100 km above Chilton (diamond). Larger dots are plotted at intervals of 15 min. Owing to the rotation of the Earth, this location tracks across the surface during the morning of the eclipse, with first contact occurring over central Ireland (square), peak eclipse over the North Wales coast (triangle) and last contact near Chester (rightmost dot). The locations of Bangor and Trelawnyd are represented by an '$\times$' and a '$*$', respectively.

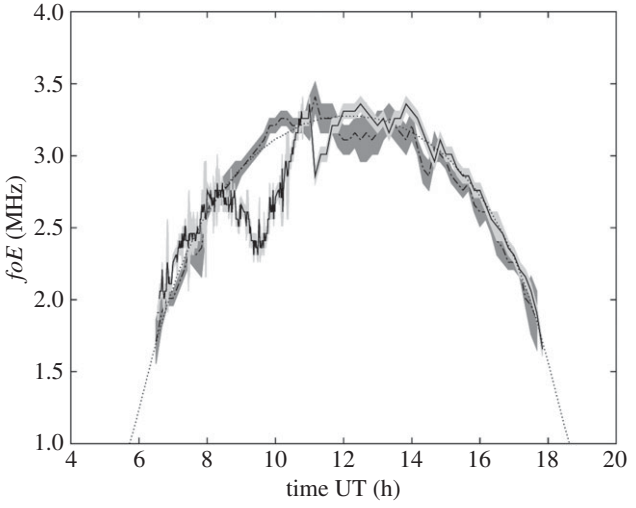

Figure 3. Time series for the E-region critical frequency, *foE*, on 20 March 2015 (day of the eclipse, solid line), the 19 March 2015 (day before the eclipse, dash-dotted line) and the modelled variation in *foE* (dotted line). Standard errors in the data are represented as light and dark grey areas around each line, respectively.

After processing, *SDO* AIA images are aligned with solar north to the top, while information about the positions of the Sun and Moon during the eclipse over Chilton was made with reference to the local zenith angle. The angle between the Sun's rotation axis and the direction of the local zenith is equal to the position angle of the solar rotation axis relative to the celestial north pole ($-25^\circ 08'$ for this epoch) minus the parallactic angle (the angle at the object between the direction to the celestial north pole and that of the zenith, measured positively eastwards).

In order to simulate the solar emissions incident on the Earth's atmosphere, the orientation of the Sun relative to the Moon was corrected for this angle and a mask was overlain on each *SDO* image to simulate the eclipse seen at 100 km above Chilton. The signal from the unobscured pixels was then summed and the fraction of the total radiation emitted at each time was calculated by dividing this value by the total signal received from the uneclipsed Sun. This process was repeated for all nine wavelengths used in this study.

Routine monitoring of the ionosphere above Chilton started in 1996 and continues the sequence started in Slough in 1932 [6]. The current ionosonde is a Digisonde [10] that is set to routinely transmit radio pulses between 1 and 20 MHz in 50 kHz steps. Such a sounding takes around three minutes to complete. In order to achieve the cadence required to track the rapid changes that occurred in the ionosphere during the eclipse, the equipment was set to transmit pulses between 1.5 and 4.5 MHz in 50 kHz steps. With such a frequency range, a cadence of 1 min was possible, with full soundings taken on the hour to enable the continuation of the long-term hourly data series. This frequency range was chosen to enable the ionospheric E-region to be studied in detail. The lower frequency was raised to 1.5 MHz since ionospheric returns are seldom received below 1.5 MHz due to the frequency response of the equipment. The E-region critical frequency, *foE*, was then manually scaled from the resulting ionograms.

3. Results

Time series for *foE* on the day of the eclipse (solid line), the day before the eclipse (dash-dotted line) and the modelled variation (dotted line) in *foE* are shown in figure 3. Uncertainties in these values are represented by the grey areas around each line. Some values of *foE* were less well defined than others due to the intermittent presence of a weak sporadic E-layer (caused by reflection from meteoric metal ions), which occasionally obscured the E-layer critical frequency.

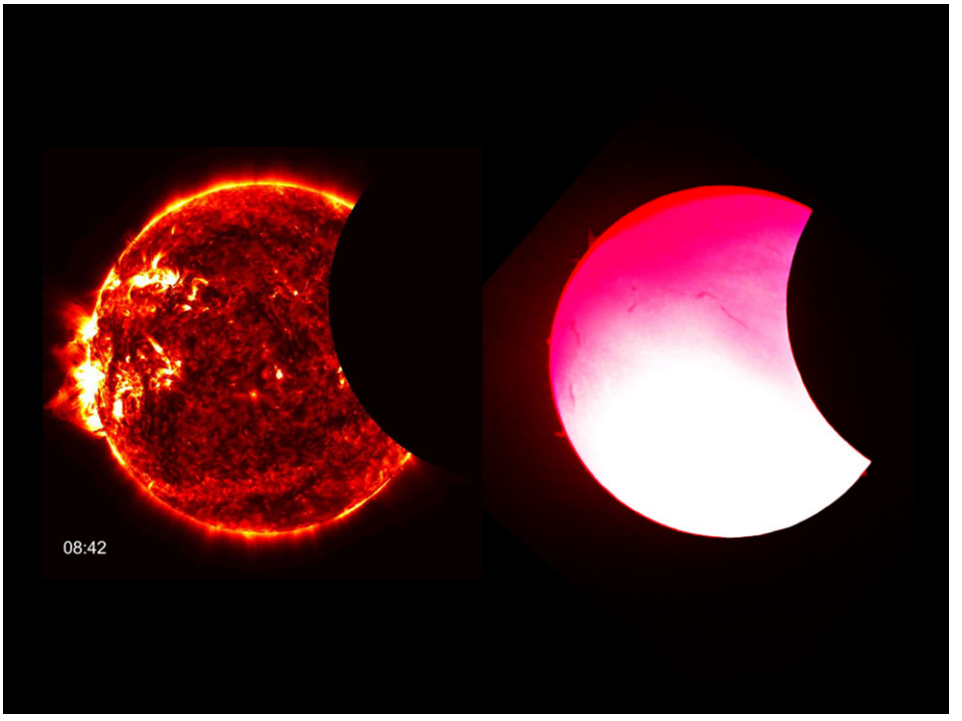

Figure 4. A comparison of the Sun observed at 171 nm by *SDO* (left panel) with an image of the eclipse as observed from Trelawnyd (right panel). The *SDO* image has been overlain with the calculated position of the moon, as observed at 100 km above Chilton. The presence of prominences and filaments in the ground-based image match features in the *SDO* image, providing useful corroboration of the coordinate transform.

The model *foE* values are generated by the Digisonde and made available in the automatically scaled data as the parameter *foEp*.

Artificial eclipse sequences were generated for each of nine *SDO* wavelengths as described above. These were then compared with images taken by observers located near the path along which the ground-based eclipse local circumstances were equivalent to those in the ionosphere above Chilton. Figure 4 presents a comparison at 8:42 UT of the Sun at 171 Å observed by the AIA instrument on *SDO* (left) with an image of the Sun in Hα as observed from Trelawnyd. The presence of prominences and filaments match those features in the *SDO* image, providing useful corroboration of the coordinate transform.

By using the modelled variation in *foE* as a control, values of Φ were estimated throughout the eclipse period. Since the modelled values make assumptions as to the expected ionizing radiation, this time sequence was scaled by a factor of 2% to ensure that the values of Φ immediately before and after the eclipse were unity, as would be expected for an uneclipsed Sun. The variation of Φ values is plotted in figure 5*a* as a dark grey line, with the standard error represented by the surrounding light grey area. Overplotted on this figure are the values of Φ estimated from the *SDO* data. The first to fourth contacts of the lunar limb with the active region over the western (right-hand) limb of the Sun are represented by vertical dotted red lines. The same for the active region on the eastern (left-hand) limb of the Sun are represented by vertical dotted blue lines. It can be seen that there is an increase in the ionospheric decay rate as the first active region is eclipsed on the western limb of the Sun, and an increase in the recovery of ionospheric densities once the second active region on the eastern limb emerges from the lunar shadow. The differences between the coronal and photospheric emissions can be clearly seen in figure 5*b*, where the time derivative of three coronal emissions most closely following the ionospheric variations (cyan,

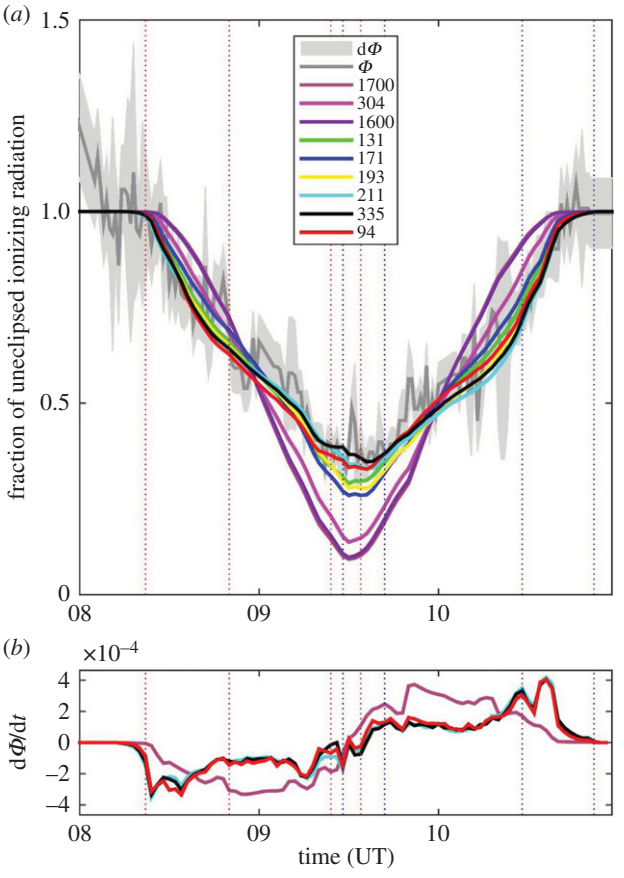

Figure 5. (*a*) The fraction of ionizing radiation incident on the ionosphere above Chilton, Φ, as a function of time (dark grey line). Standard errors in this parameter are represented by the surrounding light grey area. Overplotted on this figure are the values of Φ estimated from *SDO* data for nine of the wavelengths measured by the AIA instrument. The wavelengths are listed in the figure legend (in ångström), along with the colour of each line. Uncertainties in these *SDO*-derived parameters have been omitted for clarity but are estimated to be of the order of 1–2%. (*b*) The time derivative of the three SDO emissions that most closely matched the ionospheric variability (cyan, black and red lines corresponding to wavelengths of 211, 335 and 94 Å, respectively) compared with the time derivative of a photospheric emission (purple line, corresponding to 1700 Å). The first to fourth contacts of the lunar limb with the active region over the western (right-hand side) limb of the Sun are represented by vertical dotted red lines. The same for the active region on the eastern (left-hand side) limb of the Sun are represented by vertical dotted blue lines.

black and red lines corresponding to emissions at 211, 335 and 94 Å, respectively) are plotted alongside the time derivative of a photospheric emission (1700 Å, represented by the purple line).

As expected, the solar emissions that most closely match the ionospheric response to the eclipse are those associated with emissions from the coronal plasma. While there is localized structure in the location of the emissions on the solar disc and in the corona, the rate of change in emission at all wavelengths is generally smooth throughout the eclipse. For those emissions associated with the lower-temperature photospheric plasma, the total emission starts to decline later than other wavelengths, reaches a deeper minimum ($\Phi = 8.66\%$) and recovers sooner, as would be expected for emissions confined to, and evenly distributed across, the solar disc. These variations are more closely equivalent to the fraction of the disc occulted at any given time, with a maximum obscuration of 91.34% (compared with a predicted photospheric magnitude of 90.3% at maximum eclipse of 88.88%).

In order to see whether the artificial eclipse curves matched the ionospheric response within the expected errors, a χ^2-test was applied to the time evolution of each *SDO* wavelength compared with Φ estimated from the ionospheric data. If the two datasets match within the expected errors, the value of χ^2 will lie within $n \pm \sqrt{2n}$, where n is the number of data points. As the Φ estimated from the *SDO* data vary smoothly throughout the eclipse, their values were interpolated at the times of the ionospheric observations, giving $n = 165$ and a range of acceptable χ^2 values of 18. Errors in Φ estimated from the *SDO* data (approx. 2%) are smaller than those associated with the ionospheric data (approx. 10–20%). The Φ variations for wavelengths of 304, 1600 and 1700 Å gave $\chi^2 \gg n$, indicating that these curves do not match the ionospheric observations. For 171 Å, $\chi^2 = 192$, which is just outside the upper level of the χ^2 error range (183). All other wavelengths give χ^2 values below the lower range of expected values (147), indicating that the datasets match more closely than indicated by the expected errors. It may be that the errors associated with the ionospheric data were pessimistic given the obscuration by the underlying sporadic E-layer.

Having ascertained that the overall ionospheric response to the emissions closely followed the occultation of ionizing radiation, we then turned our attention to the small-scale variability seen in the ionosphere. With no sudden changes in solar emissions, it is clear that the remaining ionospheric variability must result from local sources of variability such as gravity waves or modulation of the sporadic E-layer by changes to the wind shear at E-region altitudes. However, an initial study of the frequency spectrum in the ionospheric data did not reveal any dominant frequencies.

4. Discussion and conclusion

While good agreement has been found between the large-scale variations in E-region ionospheric number densities and the fraction of ionizing radiation incident upon the Earth's atmosphere during the solar eclipse, it is not possible to draw any conclusions as to the possibility of identifying the occultation of specific active regions on the Sun by the ionospheric response. No sharp decreases in ionospheric response were seen since the emissions were distributed across the solar disc rather than being concentrated in a single isolated active region. In addition, the presence of a weak and intermittent sporadic E-layer served to increase the uncertainty in identifying the peak densities associated with the true E-region peak.

The results presented here do, however, provide evidence that if the ionospheric response from multiple locations were compared, these could be combined to triangulate the location of any active regions on the solar disc or localized emissions from the solar corona. Multiple ionospheric observation sites would also have the advantage that any ionospheric fluctuations due to local influences would be averaged out in the final analysis. If such an analysis were conducted for modern ionospheric data and validated against *SDO* images, the technique could then be used to investigate the localized nature of solar EUV and X-ray emissions during eclipses that were observed prior to the advent of high-altitude rockets and spacecraft. While such observations would provide only a snapshot of conditions in the solar corona, such information may help interpret any subsequent geomagnetic events and would extend our observations of solar EUV and X-ray emissions above active regions by at least a decade.

Data accessibility. Ionospheric data can be obtained through the UK Solar System Data Centre (www.ukssdc.ac.uk). Data from the *Solar Dynamics Observatory* are free to access and can be obtained via www.nasa.gov/sdo. Information on the ground-based local circumstances for the eclipse can be obtained via www.eclipse.org managed by S. A. Bell at H.M. Nautical Almanac Office. Specific calculations on the local circumstances at ionospheric heights were provided by S. A. Bell. For information about the ground-based solar images, contact the North Wales Astronomy Society. Data analysis was carried out by C. J. Scott using MATLAB. Code is available upon request from chris.scott@reading.ac.uk.

Authors' contributions. C.J.S. helped design the experiment, led the data analysis and produced the first draft of the paper. J.B. helped design the experiment, collected and provided the ionospheric measurements. S.A.B. calculated local circumstances for the eclipse. J.W. carried out image processing of the ground-based solar

images and contributed to the data analysis. L.A.B. contributed to the data analysis with particular emphasis on the spacecraft data. D.S. and S.T. carried out ground-based measurements of the solar eclipse. All authors contributed to the production and revision of the manuscript.

Competing interests. We have no competing interests.

Funding. L.B. is currently funded under STFC grant number ST/M000885/1.

Acknowledgements. Data from the *Solar Dynamics Observatory* are made available by courtesy of NASA/SDO and the AIA, EVE and HMI science teams. Ionospheric data have been made available by courtesy of the UK Solar System Data Centre (www.ukssdc.ac.uk). The authors thank members of the North Wales Astronomy Society for their participation in this experiment.

References

1. Beynon WJG, Brown GM. 1956 *Solar eclipses and the ionosphere*. London, UK: Pergamon Press.
2. Minnis CM. 1956 The origin of the E- and F1-layer ionizing radiation, solar eclipses and the ionosphere. *J. Atmos. Terrest. Phys.* **6** (Suppl.).
3. Davis CJ, Lockwood M, Bell SA, Smith JA, Clarke EM. 2000 Ionospheric measurements of relative coronal brightness during the total solar eclipses of 11 August, 1999 and 9 July, 1945. *Ann. Geophys.* **18**, 182–190. (doi:10.1007/s00585-000-0182-z)
4. Davis CJ, Clarke EM, Bamford RA, Lockwood M, Bell SA. 2001 Long term changes in EUV and X-ray emissions from the solar corona and chromosphere as measured by the response of the Earth's ionosphere during total solar eclipses from 1932 to 1999. *Ann. Geophys.* **19**, 263–273. (doi:10.5194/angeo-19-263-2001)
5. Davis CJ, Bell SA, Stamper R, Poole AWV, McKinnell LA, Wilkinson P. 2009 A potential lag between the open solar magnetic source flux and solar EUV and X-ray emissions as measured by the Earth's ionosphere during total solar eclipses. *Ann. Geophys.* **27**, 2449–2456. (doi:10.5194/angeo-27-2449-2009)
6. Pesnell WD, Thompson BJ, Chamberlin PC. 2012 The *Solar Dynamics Observatory* (*SDO*). *Solar Phys.* **275**, 3–15. (doi:10.1007/s11207-011-9841-3)
7. Gardiner GW, Lane JA, Rishbeth H. 1982 Radio and space research at Slough 1920–1981. *Radio Electron. Eng.* **52**, 111–121. (doi:10.1049/ree.1982.0015)
8. Schunk RW, Nagy AF. 2000 *Ionospheres: physics, plasma physics and chemistry*. Cambridge, UK: Cambridge University Press.
9. Lemen JR *et al.* 2012 The Atmospheric Imaging Assembly (AIA) on the *Solar Dynamics Observatory* (*SDO*). *Solar Phys.* **275**, 17–40. (doi:10.1007/s11207-011-9776-8)
10. Bibl K, Reinisch BW. 1978 The universal digital ionosonde. *Radio Sci.* **13**, 519–530. (doi:10.1029/RS013i003p00519)